

A search for sterile neutrinos mixing with muon neutrinos in MINOS

P. Adamson,⁸ I. Anghel,^{15, 1} A. Aurisano,⁷ G. Barr,²² M. Bishai,³ A. Blake,^{5, 16} G. J. Bock,⁸ D. Bogert,⁸ S. V. Cao,³⁰ T. J. Carroll,³⁰ C. M. Castromonte,⁹ R. Chen,¹⁸ S. Childress,⁸ J. A. B. Coelho,³¹ L. Corwin,^{14, *} D. Cronin-Hennessy,¹⁹ J. K. de Jong,²² S. De Rijck,³⁰ A. V. Devan,³³ N. E. Devenish,²⁸ M. V. Diwan,³ C. O. Escobar,⁶ J. J. Evans,¹⁸ E. Falk,²⁸ G. J. Feldman,¹⁰ W. Flanagan,³⁰ M. V. Frohne,^{11, †} M. Gabrielyan,¹⁹ H. R. Gallagher,³¹ S. Germani,¹⁷ R. A. Gomes,⁹ M. C. Goodman,¹ P. Gouffon,²⁵ N. Graf,²³ R. Gran,²⁰ K. Grzelak,³² A. Habig,²⁰ S. R. Hahn,⁸ J. Hartnell,²⁸ R. Hatcher,⁸ A. Holin,¹⁷ J. Huang,³⁰ J. Hylen,⁸ G. M. Irwin,²⁷ Z. Isvan,³ C. James,⁸ D. Jensen,⁸ T. Kafka,³¹ S. M. S. Kasahara,¹⁹ G. Koizumi,⁸ M. Kordosky,³³ A. Kreymer,⁸ K. Lang,³⁰ J. Ling,³ P. J. Litchfield,^{19, 24} P. Lucas,⁸ W. A. Mann,³¹ M. L. Marshak,¹⁹ N. Mayer,³¹ C. McGivern,²³ M. M. Medeiros,⁹ R. Mehdiyev,³⁰ J. R. Meier,¹⁹ M. D. Messier,¹⁴ W. H. Miller,¹⁹ S. R. Mishra,²⁶ S. Moed Sher,⁸ C. D. Moore,⁸ L. Mualem,⁴ J. Musser,¹⁴ D. Naples,²³ J. K. Nelson,³³ H. B. Newman,⁴ R. J. Nichol,¹⁷ J. A. Nowak,^{19, †} J. O'Connor,¹⁷ M. Orchanian,⁴ R. B. Pahlka,⁸ J. Paley,¹ R. B. Patterson,⁴ G. Pawloski,¹⁹ A. Perch,¹⁷ M. M. Pfützner,¹⁷ D. D. Phan,³⁰ S. Phan-Budd,¹ R. K. Plunkett,⁸ N. Poonthottathil,⁸ X. Qiu,²⁷ A. Radovic,³³ B. Rebel,⁸ C. Rosenfeld,²⁶ H. A. Rubin,¹³ P. Sail,³⁰ M. C. Sanchez,^{15, 1} J. Schneps,³¹ A. Schreckenberger,³⁰ P. Schreiner,¹ R. Sharma,⁸ A. Sousa,⁷ N. Tagg,²¹ R. L. Talaga,¹ J. Thomas,¹⁷ M. A. Thomson,⁵ X. Tian,²⁶ A. Timmons,¹⁸ J. Todd,⁷ S. C. Tognini,⁹ R. Toner,¹⁰ D. Torretta,⁸ G. Tzanakos,^{2, †} J. Urheim,¹⁴ P. Vahle,³³ B. Viren,³ A. Weber,^{22, 24} R. C. Webb,²⁹ C. White,¹³ L. Whitehead,¹² L. H. Whitehead,¹⁷ S. G. Wojcicki,²⁷ and R. Zwaska⁸

(The MINOS Collaboration)

¹Argonne National Laboratory, Argonne, Illinois 60439, USA

²Department of Physics, University of Athens, GR-15771 Athens, Greece

³Brookhaven National Laboratory, Upton, New York 11973, USA

⁴Lauritsen Laboratory, California Institute of Technology, Pasadena, California 91125, USA

⁵Cavendish Laboratory, University of Cambridge, Cambridge CB3 0HE, United Kingdom

⁶Universidade Estadual de Campinas, IFGW, CP 6165, 13083-970, Campinas, SP, Brazil

⁷Department of Physics, University of Cincinnati, Cincinnati, Ohio 45221, USA

⁸Fermi National Accelerator Laboratory, Batavia, Illinois 60510, USA

⁹Instituto de Física, Universidade Federal de Goiás, 74690-900, Goiânia, GO, Brazil

¹⁰Department of Physics, Harvard University, Cambridge, Massachusetts 02138, USA

¹¹Holy Cross College, Notre Dame, Indiana 46556, USA

¹²Department of Physics, University of Houston, Houston, Texas 77204, USA

¹³Department of Physics, Illinois Institute of Technology, Chicago, Illinois 60616, USA

¹⁴Indiana University, Bloomington, Indiana 47405, USA

¹⁵Department of Physics and Astronomy, Iowa State University, Ames, Iowa 50011 USA

¹⁶Lancaster University, Lancaster, LA1 4YB, UK

¹⁷Department of Physics and Astronomy, University College London, London WC1E 6BT, United Kingdom

¹⁸School of Physics and Astronomy, University of Manchester, Manchester M13 9PL, United Kingdom

¹⁹University of Minnesota, Minneapolis, Minnesota 55455, USA

²⁰Department of Physics, University of Minnesota Duluth, Duluth, Minnesota 55812, USA

²¹Otterbein University, Westerville, Ohio 43081, USA

²²Subdepartment of Particle Physics, University of Oxford, Oxford OX1 3RH, United Kingdom

²³Department of Physics and Astronomy, University of Pittsburgh, Pittsburgh, Pennsylvania 15260, USA

²⁴Rutherford Appleton Laboratory, Science and Technology Facilities Council, Didcot, OX11 0QX, United Kingdom

²⁵Instituto de Física, Universidade de São Paulo, CP 66318, 05315-970, São Paulo, SP, Brazil

²⁶Department of Physics and Astronomy, University of South Carolina, Columbia, South Carolina 29208, USA

²⁷Department of Physics, Stanford University, Stanford, California 94305, USA

²⁸Department of Physics and Astronomy, University of Sussex, Falmer, Brighton BN1 9QH, United Kingdom

²⁹Physics Department, Texas A&M University, College Station, Texas 77843, USA

³⁰Department of Physics, University of Texas at Austin, Austin, Texas 78712, USA

³¹Physics Department, Tufts University, Medford, Massachusetts 02155, USA

³²Department of Physics, University of Warsaw, PL-02-093 Warsaw, Poland

³³Department of Physics, College of William & Mary, Williamsburg, Virginia 23187, USA

(Dated: October 9, 2022)

We report results of a search for oscillations involving a light sterile neutrino over distances of 1.04 km and 735 km in a ν_μ -dominated beam with peak energy of 3 GeV. The data, from an exposure of 10.56×10^{20} protons-on-target, are analyzed using a phenomenological model with one sterile neutrino. We constrain the mixing parameters θ_{24} and Δm_{41}^2 and set limits on parameters of

the four-dimensional PMNS matrix, $|U_{\mu 4}|^2$ and $|U_{\tau 4}|^2$, under the assumption that mixing between ν_e and ν_s is negligible ($|U_{e4}|^2 = 0$). No evidence for $\nu_\mu \rightarrow \nu_s$ transitions is found and we set a world-leading limit on θ_{24} for values of $\Delta m_{41}^2 \lesssim 1 \text{ eV}^2$.

PACS numbers: 14.60.Pq, 14.60.Lm, 29.27.-a

Studies of neutrinos and antineutrinos produced in the Sun, the atmosphere, and by reactors and accelerators [1] have established that neutrinos have mass and that the weak-interaction flavor eigenstates, ν_ℓ ($\ell = e, \mu, \tau$), are related to the mass eigenstates, ν_i ($i = 1, 2, 3$), by a mixing matrix, U :

$$|\nu_\ell\rangle = \sum_i U_{\ell i} |\nu_i\rangle. \quad (1)$$

Measurements of the shape of the Z -boson resonance [2] show that there are three active neutrino flavors with masses less than $m_Z/2$. The standard picture of neutrino mixing therefore assumes U is a 3×3 matrix, the PMNS matrix [3–5], that relates the flavor states to three neutrino mass states, m_1 , m_2 and m_3 . The matrix is commonly parametrized using three mixing angles, θ_{12} , θ_{23} and θ_{13} , and a charge-parity (CP) violating phase δ [6]. The three angles and the two mass splittings, $\Delta m_{21}^2 = m_2^2 - m_1^2$ and $|\Delta m_{32}^2| = |m_3^2 - m_2^2|$, have been measured in multiple experiments [1].

The three-flavor model of neutrino mixing provides an excellent description of most, but not all, neutrino data. In particular, LSND observed a 3.8σ excess consistent with $\bar{\nu}_\mu \rightarrow \bar{\nu}_e$ oscillations driven by a mass splitting $0.2 \leq \Delta m^2 \leq 10 \text{ eV}^2$ that is incompatible with Δm_{21}^2 or Δm_{32}^2 [7]. MiniBooNE searched for oscillations in the same range of mass splittings using beams of ν_μ and $\bar{\nu}_\mu$ and found 3.4σ and 2.8σ excesses of ν_e and $\bar{\nu}_e$, respectively [8].

Many experiments have measured $\bar{\nu}_e$ fluxes from reactors at short baselines of 10–1000 m. A recent calculation [9, 10] predicts a flux that is about 3% larger than previously assumed. The data display a deficit with respect to that prediction, the “reactor anomaly”, which can be interpreted as $\bar{\nu}_e$ disappearance due to oscillations with $\Delta m^2 \gtrsim 0.1 \text{ eV}^2$ [11]. Finally, a deficit of ν_e has been observed from the gallium calibration sources of SAGE and GALLEX [12, 13] which, when interpreted as oscillations, is consistent with the Δm^2 range favored by the reactor anomaly.

The anomalous oscillation signals described above may potentially be reconciled with data supporting the three-flavor oscillation picture by the addition of one or more sterile neutrinos that do not experience the weak interaction, but which mix with the active neutrinos [14]. Since neutrinos have mass, sterile states may naturally arise from extensions to the Standard Model [15]. In this Letter, we test a phenomenological model in which the PMNS matrix is extended by the addition of a fourth neutrino mass eigenstate, ν_4 , and a single sterile flavor state,

ν_s . This ‘3+1’ phenomenological model introduces three new mixing angles, θ_{14} , θ_{24} and θ_{34} , and two additional phases, δ_{14} and δ_{24} , when parameterized as in [6]. In this nomenclature the PMNS phase $\delta \equiv \delta_{13}$ and all δ_{ij} -dependent terms appear multiplied by the corresponding $\sin \theta_{ij}$ in U . In the following discussion we denote individual elements of U as U_{li} with $l = e, \mu, \tau, s$ and $i = 1 \dots 4$. We also write $c_{ij} = \cos \theta_{ij}$, $s_{ij} = \sin \theta_{ij}$, and $\Delta_{ji} = \frac{\Delta m_{ji}^2 L}{4E_\nu}$, where $\Delta m_{ji}^2 \equiv m_j^2 - m_i^2$, L is the distance traveled by the neutrino, and E_ν is the neutrino energy.

The MiniBooNE and LSND experiments were conducted at $L/E_\nu \sim 1 \text{ km}/\text{GeV}$, a parameter space in which $\sin^2 \Delta_{32} \sim 10^{-5}$ and $\sin^2 \Delta_{21} \sim 10^{-8}$, rendering oscillations due to Δm_{32}^2 and Δm_{21}^2 negligible. In this case, and assuming $|\Delta m_{41}^2| \gg |\Delta m_{32}^2| > |\Delta m_{21}^2|$, the ν_e appearance probability is

$$P(\nu_\mu \rightarrow \nu_e) = 4|U_{\mu 4}|^2 |U_{e4}|^2 \sin^2 \Delta_{41}, \quad (2)$$

where $|U_{\mu 4}| = c_{14} s_{24}$ and $|U_{e4}| = s_{14}$. Reactor experiments study $\bar{\nu}_e \rightarrow \bar{\nu}_e$ and have placed stringent limits on θ_{14} [16, 17].

MINOS measures neutrino oscillations using ν_μ charged-current (CC) and neutral-current (NC) interactions in a Far Detector (FD) and a Near Detector (ND) separated by 734 km [18, 19]. The neutrinos are produced by directing protons with energies of 120 GeV from the Fermilab Main Injector onto a graphite target, located 1.04 km upstream of the ND, producing π and K mesons. These mesons are focused by magnetic horns before decaying in a 675 m long tunnel to produce predominantly muon-type neutrinos [20]. The ranges of L/E probed by the two MINOS detectors are shown in Fig. 1. Disappearance of ν_μ occurs with a probability

$$P(\nu_\mu \rightarrow \nu_\mu) = 1 - 4 \sum_{i=1}^4 \sum_{j>i}^4 |U_{\mu i}|^2 |U_{\mu j}|^2 \sin^2 \Delta_{ji}. \quad (3)$$

In the analysis presented in this Letter, we use the exact oscillation probability to extract limits on the parameters. In the following discussion of the phenomenology, for simplicity we only show leading terms.

Terms in Δ_{21} are negligible, and we can approximate $\Delta m_{32}^2 \approx \Delta m_{31}^2$. In the limit $\Delta m_{41}^2 \gg \Delta m_{31}^2$ we can also approximate $\Delta m_{43}^2 \approx \Delta m_{42}^2 \approx \Delta m_{41}^2$ and expand the oscillation probability to second order in the small terms s_{13} , s_{14} , s_{24} and $\cos 2\theta_{23}$, yielding

$$P(\nu_\mu \rightarrow \nu_\mu) \approx 1 - \sin^2 2\theta_{23} \cos 2\theta_{24} \sin^2 \Delta_{31} - \sin^2 2\theta_{24} \sin^2 \Delta_{41}. \quad (4)$$

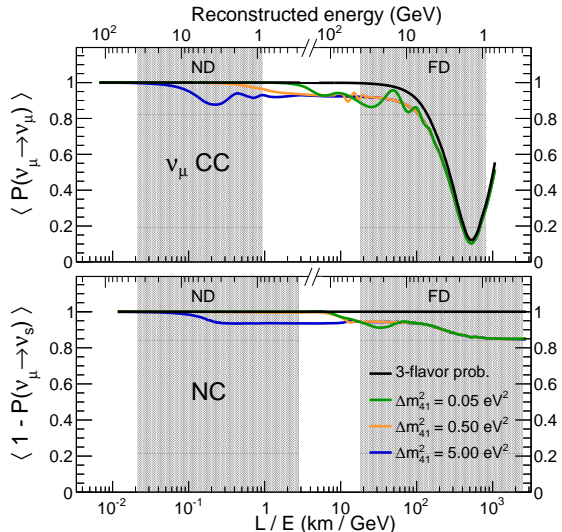


FIG. 1. Muon neutrino oscillation probabilities as a function of L/E , where L is the distance traveled by the neutrinos, and E is the reconstructed neutrino energy (top horizontal axis of each panel), for three different values of Δm_{41}^2 , with $\theta_{14} = 0.15$, $\theta_{24} = 0.2$, $\theta_{34} = 0.5$, and values of Δm_{31}^2 , Δm_{21}^2 , θ_{12} , θ_{23} and θ_{13} from [1]. The dip in $P(\nu_\mu \rightarrow \nu_\mu)$ at 500 km/GeV is due to oscillations driven by Δm_{31}^2 . The grey bands indicate the regions of reconstructed energy where CC ν_μ interactions (top panel) and NC interactions (bottom panel) are observed in the two detectors.

Thus, mixing with sterile neutrinos in the MINOS CC ν_μ sample is controlled by θ_{24} and would be seen as a depletion of events for $\Delta_{41} \gtrsim \pi/2$, as shown in the top panel of Fig. 1.

For $10^{-3} \text{ eV}^2 \lesssim \Delta m_{41}^2 \lesssim 0.1 \text{ eV}^2$ an energy-dependent depletion would be observed at the FD with no effect at the ND. The $\Delta m_{41}^2 = 0.05 \text{ eV}^2$ curve in the top panel of Fig. 1 shows an example of this behavior. As Δm_{41}^2 increases toward 1 eV^2 we have $\Delta_{41} \gg \pi/2$ at the FD. In this case – the fast-oscillation regime – an energy-independent reduction in the event rate would be observed, since $\sin^2 \Delta_{41} \rightarrow 1/2$ when the finite energy resolution of the detectors is considered. The $\Delta m_{41}^2 = 0.50 \text{ eV}^2$ curve in the top panel of Fig. 1 shows an example of fast oscillations. For $\Delta m_{41}^2 \gtrsim 1 \text{ eV}^2$ an additional energy-dependent depletion of ν_μ would be seen at the ND, with the energy of maximum oscillation increasing with Δm_{41}^2 . An example of these ND oscillations is shown by the $\Delta m_{41}^2 = 5.00 \text{ eV}^2$ curve in the top panel of Fig. 1. For $\Delta m_{41}^2 \gtrsim 100 \text{ eV}^2$ fast oscillations occur at both detectors.

MINOS is also sensitive to sterile neutrinos via the disappearance of NC events [21–23], as shown in the bottom panel of Fig. 1, which would occur with a probability

$$1 - P(\nu_\mu \rightarrow \nu_s) \approx 1 - c_{14}^4 c_{34}^2 \sin^2 2\theta_{24} \sin^2 \Delta_{41} - A \sin^2 \Delta_{31} - B \sin 2\Delta_{31}. \quad (5)$$

The terms A and B are functions of the mixing an-

gles and phases. To first order, $A = s_{34}^2 \sin^2 2\theta_{23}$ and $B = \frac{1}{2} \sin \delta_{24} s_{24} \sin 2\theta_{34} \sin 2\theta_{23}$. The NC sample is therefore sensitive to θ_{34} and δ_{24} in addition to θ_{24} , although that sensitivity is limited by poor neutrino-energy resolution (due to the undetected outgoing neutrino), a lower event rate due to cross-sections, and ν_μ and ν_e CC backgrounds.

The MINOS apparatus and NuMI beam have been described in detail elsewhere [20, 24]. We analyze an exposure of 10.56×10^{20} protons-on-target (POT) used to produce a ν_μ -dominated beam with a peak energy of 3 GeV. The detectors are magnetized steel-scintillator, tracking-sampling calorimeters that utilize an average field of 1.3 T to measure the charge and momentum of muons. The energy of hadronic showers is measured using calorimetry. In the case of CC ν_μ interactions, this is combined with topological information through a k -Nearest-Neighbor (k NN) algorithm [25].

A sample of NC-enhanced events is isolated by searching for interactions that induce activity spread over fewer than 47 steel-scintillator planes. Events with a reconstructed track are required to penetrate no more than five detector planes beyond the end of the hadronic shower. Additional selection requirements are imposed in the ND to remove cases in which the reconstruction program was confused by multiple coincident events. The selected NC sample in the ND has an efficiency of 79.9% and a purity of 58.9%, both estimated from Monte Carlo (MC) simulation. The background is composed of 86.9% CC ν_μ interactions and 13.1% CC ν_e interactions. At the FD, assuming standard three-flavor oscillations, the efficiency of the sample is 87.6% and the purity is 61.3%, with the backgrounds comprising 73.8% CC ν_μ interactions, 21.6% CC ν_e interactions and 4.6% CC ν_τ interactions. A lower bound on the energy of the incident neutrino is estimated from the energy of the hadronic recoil system, with a mean resolution of 41.7% on the energy of the recoil system in the FD.

We isolate a sample of CC ν_μ ($\nu_\mu N \rightarrow \mu X$) events by searching for interactions inside our detectors with a single outgoing μ track and possible hadronic activity from the recoil system X . We discriminate between CC and NC events by combining four topological variables describing track properties into a single discriminant variable, using a k NN algorithm [26]. Events are required to have failed the NC selection procedure to be included in the CC ν_μ sample. In the ND, the selected CC sample has an efficiency of 53.9% and a purity of 98.7%, both estimated from MC simulation. At the FD, assuming three-flavor oscillations, the corresponding efficiency is 84.6% and the purity is 99.1%. The neutrino energy is reconstructed by summing the energies of the muon and hadronic showers, with a mean resolution of 17.3% in the FD.

MINOS oscillation analyses have traditionally used the CC and NC neutrino energy spectra measured by the ND

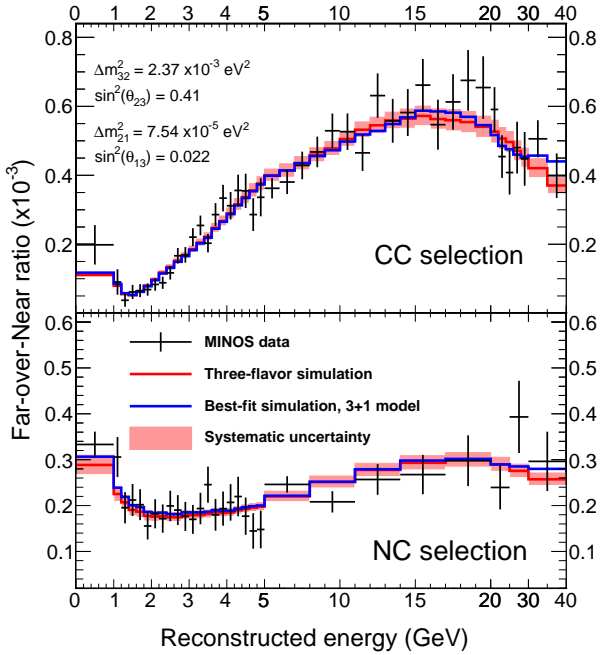


FIG. 2. The ratios of the energy spectra in the Far Detector to those in the Near Detector, shown for the CC ν_μ (top) and NC (bottom) samples. The solid lines represent the predicted ratios from fits to the standard three-flavor oscillation model and to the 3+1 sterile neutrino model.

to predict the spectra at the FD as a function of oscillation parameters [27]. However, the sterile oscillation parameter space to which MINOS is sensitive stretches over the range $10^{-3} \text{ eV}^2 \lesssim \Delta m^2 \lesssim 10^2 \text{ eV}^2$, which could cause oscillations to impact both detectors [28]. Therefore, instead of using the ND data to predict the FD energy spectra, we analyze the ratio of energy spectra observed in the FD to those observed in the ND. This Far-over-Near ratio is analyzed for both CC ν_μ and NC events, as shown in Fig. 2. Aside from the overall difference in the number of events (caused by the distance between the detectors, their different masses and efficiencies, and the beam divergence) the main effect is the energy-dependent suppression of events at the FD caused by oscillations driven by Δm^2_{32} . Our analysis searches for modulations on top of that oscillation pattern, caused by the sterile sector, by minimizing the χ^2 as a function of the oscillation parameters:

$$\chi^2_{CC,NC} = \sum_{m=1}^N \sum_{n=1}^N (x_m - \mu_m)(V^{-1})_{mn}(x_n - \mu_n) + \text{const.} \quad (6)$$

Here, we denote the measured Far-over-Near ratio as x_m , where $m = 1 \dots N$ labels N energy bins between 0 and 40 GeV. The predicted ratio is denoted μ_m . The dependence of μ_m on the oscillation parameters is taken

from an MC simulation that includes the full range of experimental effects, and uses an exact form of all oscillation probabilities in vacuum with no approximations. In Eq. (6), V is an $N \times N$ covariance matrix expressing the combined statistical and systematic uncertainty on $\vec{\mu}$. For very high $\Delta m^2_{41} \gtrsim 50 \text{ eV}^2$, both detectors are in the fast-oscillation limit and the only sensitivity comes from the overall rate measured in one of the two detectors. To account for the uncertainty on the overall rate we add a term $\chi^2_{\text{rate}} = \frac{(X - M)^2}{\sigma_M^2}$, where X and M are the total number of ND events measured and simulated, respectively, and σ_M is the uncertainty on M , which is conservatively assigned a value of 50%, reflecting the fact that most measurements of neutrino fluxes and cross sections assume only three neutrino flavors.

We fit for θ_{23} , θ_{24} , θ_{34} , Δm^2_{32} and Δm^2_{41} , and hold all other parameters fixed. We set $\sin^2 \theta_{12} = 0.307$ and $\Delta m^2_{21} = 7.54 \times 10^{-5} \text{ eV}^2$ based on a global fit to neutrino data [29], and $\sin^2 \theta_{13} = 0.022$ based on a weighted average of recent results from reactor experiments [30–32]. An analysis of solar and reactor neutrino data yields the constraint $\sin^2 \theta_{14} = |U_{e4}|^2 < 0.041$ at 90% C.L. [33], which is small enough to have a negligible effect on this analysis, so we set $\theta_{14} = 0$. This analysis has negligible sensitivity to δ_{13} and δ_{14} , and minimal sensitivity to δ_{24} , hence all are set to zero. The impact of including the matter potential in the oscillation probability was investigated and found to have a negligible effect. The neutrino path-length between the meson decay point and the ND was taken into account in the computation of oscillation probabilities.

Figure 2 shows a good agreement between the measured Far-over-Near ratios and those predicted using a three-flavor hypothesis. No significant distortions indicative of sterile neutrinos are observed. The predicted ratios include both statistical and systematic uncertainties that are incorporated into Eq. (6) via a covariance matrix,

$$V = V_{\text{stat}} + V_{\text{norm}} + V_{\text{acc}} + V_{\text{NC}} + V_{\text{other}}, \quad (7)$$

where the terms account for the various sources of uncertainty. Figure 3 shows the effects that the sources of systematic uncertainty have on the sensitivity of the sterile neutrino search. We describe each source of uncertainty below.

V_{stat} contains the statistical uncertainty, which is less than 24% in each energy bin and 15% on average. V_{norm} contains a 1.6% uncertainty in the relative normalization of the CC sample between the ND and FD, and a corresponding 2.2% uncertainty for the NC sample. This accounts for uncertainties in reconstruction efficiencies, and was determined by a scanning study.

V_{acc} accounts for uncertainties on the acceptance and selection efficiency of the ND. These uncertainties were evaluated by varying event-selection requirements in data

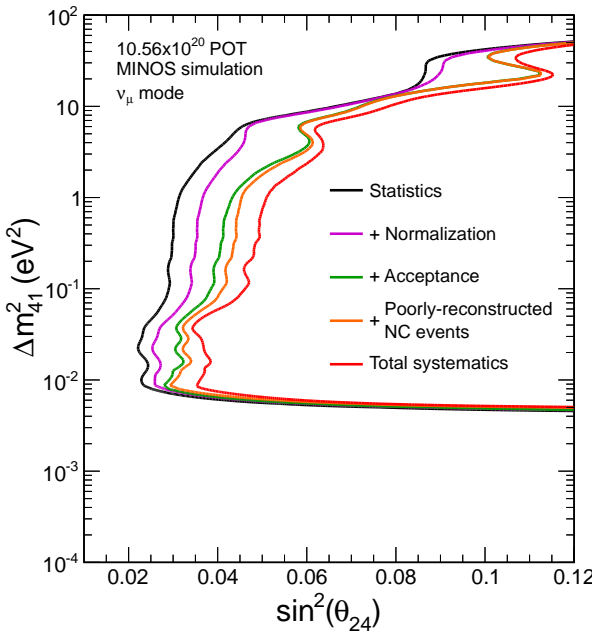


FIG. 3. The effects of systematic uncertainties on the 90% C.L. sensitivity in the $(\sin^2 \theta_{24}, \Delta m^2_{41})$ plane, shown by successive inclusion of the listed uncertainties.

and MC simulation to probe known weaknesses in the simulation. As these requirements were varied, the total variations in the ND data to MC ratios were taken as systematic uncertainties on the Far-over-Near ratios. The total uncertainty included in V_{acc} , which is energy-dependent and includes correlations between different bins, varies from 2% to 6% for the CC sample and is below 0.6% at all energies for the NC sample.

V_{NC} accounts for an uncertainty on the procedure used to remove poorly-reconstructed events from the NC sample. The variables used to identify such poorly-reconstructed events are not perfectly modeled by the MC simulation. A procedure, described in [34], assesses an uncertainty arising from this mismodeling. The total uncertainty, which includes correlations between energy bins, falls from 5% below 1 GeV to less than 1.5% above 5 GeV.

V_{other} includes terms to account for all sources of uncertainty in neutrino interaction cross sections and the flux of neutrinos produced in the NuMI beam. The total uncertainty on the FD to ND ratios arising from these sources is no more than 4% in any parts of the energy spectra.

We fit the 3 + 1 model to the data by dividing the $(\sin^2 \theta_{24}, \Delta m^2_{41})$ plane into fine bins and minimizing Eq. (6) in each bin with respect to Δm^2_{32} , θ_{23} , and θ_{34} . At each point in the plane we interpret the significance of the $\Delta\chi^2$ with respect to the global minimum accord-

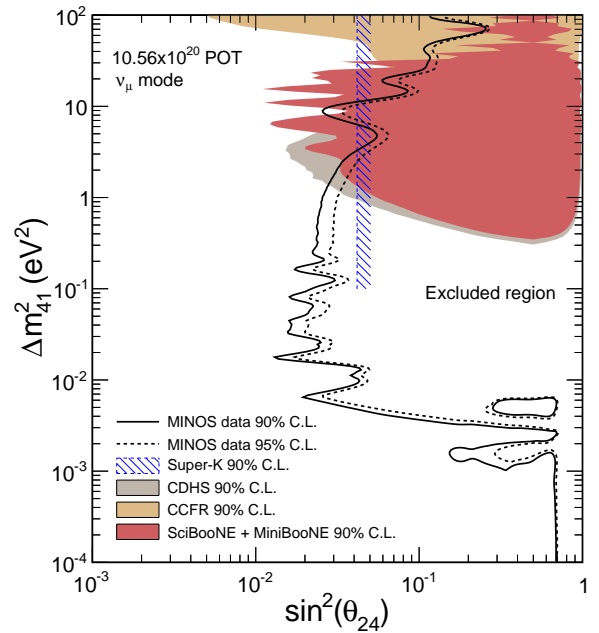


FIG. 4. The MINOS 90% and 95% confidence limits in the $(\sin^2 \theta_{24}, \Delta m^2_{41})$ plane compared with results from previous experiments [36–39]. The areas to the right of the MINOS lines are excluded at their respective confidence levels.

ing to the unified procedure of Feldman and Cousins [35]. In this procedure, MC pseudo-experiments are generated, with bin-to-bin statistical and systematic fluctuations incorporated by sampling from a multi-dimensional Gaussian with covariance matrix V (defined in Eq. (7)). The result is shown in Fig. 4, with the area to the right of the curves excluded at their respective confidence limits. The data are consistent with three-flavor oscillations at 54.7% C.L.; no evidence for sterile neutrinos is observed. The world's best limit on $\sin^2 \theta_{24}$ is established for $\Delta m^2_{41} < 1 \text{ eV}^2$, a largely unmeasured region of parameter space.

For $\Delta m^2_{41} < 10^{-2} \text{ eV}^2$ it becomes possible for one of the three mass splittings, Δm^2_{41} , Δm^2_{42} or Δm^2_{43} , to match the scale of oscillations in the Δm^2_{32} sector. This results in solutions that are degenerate with the standard three-flavor prediction, creating an island of allowed parameter space that is visible in Fig. 4.

Upper limits on the angles θ_{24} and θ_{34} , which correspond to limits on elements of the PMNS matrix, may be defined at fixed values of Δm^2_{41} . For $\Delta m^2_{41} = 0.5 \text{ eV}^2$, the data constrain $\sin^2 \theta_{24} < [0.016 \text{ (90\% C.L.)}, 0.022 \text{ (95\% C.L.)}]$; under the assumption that $|U_{e4}|^2 = 0$, these are also limits on $|U_{\mu 4}|^2 = c_{14}^2 s_{24}^2$. For $\Delta m^2_{41} = 0.5 \text{ eV}^2$, the data also constrain $\sin^2 \theta_{34} < [0.20 \text{ (90\% C.L.)}, 0.28 \text{ (95\% C.L.)}]$; under the assumption $c_{14}^2 = c_{24}^2 = 1$, these are also limits on

$$|U_{\tau 4}|^2 = c_{14}^2 c_{24}^2 s_{34}^2.$$

In conclusion, we have used samples of CC ν_μ and NC interactions from the NuMI neutrino beam to place a constraint on the existence of sterile neutrinos. We use a 3 + 1 model to quantify this constraint, and are sensitive to a range of Δm_{41}^2 covering almost five orders in magnitude. Over much of this region, we place the first constraints on the mixing angle θ_{24} . In an accompanying Letter [40], we present a combination of this constraint with those on θ_{14} from the Daya Bay [16] and Bugey [17] reactor experiments to set a limit that is directly comparable with the possible hints of sterile neutrinos seen by the LSND and MiniBooNE experiments.

This work was supported by the U.S. DOE; the U.K. STFC; the U.S. NSF; the State and University of Minnesota; and Brazil's FAPESP, CNPq and CAPES. We are grateful to the Minnesota Department of Natural Resources and the personnel of the Soudan Laboratory and Fermilab. We thank the Texas Advanced Computing Center at The University of Texas at Austin for the provision of computing resources. We thank A. Smirnov and C. Giunti for useful discussions.

* Now at South Dakota School of Mines and Technology, Rapid City, South Dakota 57701, USA.
 † Deceased.
 ‡ Now at Lancaster University, Lancaster, LA1 4YB, UK.
 [1] K. A. Olive *et al.* (Particle Data Group), Chin. Phys. C **38**, 090001 (2014), see the review on neutrino mass, mixing, and oscillations.
 [2] S. Schael *et al.* (ALEPH, DELPHI, L3, OPAL, SLD, LEP Electroweak Working Group, SLD Electroweak and Heavy Flavour Groups), Phys. Rept. **427**, 257 (2006).
 [3] Z. Maki, M. Nakagawa, and S. Sakata, Prog. Theor. Phys. **28**, 870 (1962).
 [4] B. Pontecorvo, Sov. Phys. JETP **26**, 984 (1968).
 [5] V. N. Gribov and B. Pontecorvo, Phys. Lett. B **28**, 493 (1969).
 [6] H. Harari and M. Leurer, Phys. Lett. B **181**, 123 (1986).
 [7] A. Aguilar *et al.* (LSND), Phys. Rev. D **64**, 112007 (2001).
 [8] A. A. Aguilar-Arevalo *et al.* (MiniBooNE), Phys. Rev. Lett. **110**, 161801 (2013).
 [9] Th. A. Mueller *et al.*, Phys. Rev. C **83**, 054615 (2011).
 [10] P. Huber, Phys. Rev. C **84**, 024617 (2011).
 [11] G. Mention *et al.*, Phys. Rev. D **83**, 073006 (2011).

[12] M. A. Acero, C. Giunti, and M. Laveder, Phys. Rev. D **78**, 073009 (2008).
 [13] C. Giunti and M. Laveder, Phys. Rev. C **83**, 054615 (2011).
 [14] S. Gariazzo *et al.*, J. Phys. G **43**, 033001 (2016).
 [15] R. R. Volkas, Prog. Part. Nucl. Phys. **48**, 161 (2002).
 [16] F. P. An *et al.* (Daya Bay), (2016), submitted to Phys. Rev. Lett., arXiv:1607.01174 [hep-ex].
 [17] B. Achkar *et al.* (Bugey), Nucl. Phys. B **434**, 503 (1995).
 [18] P. Adamson *et al.* (MINOS), Phys. Rev. Lett. **112**, 191801 (2014).
 [19] P. Adamson *et al.* (MINOS), Phys. Rev. Lett. **110**, 251801 (2013).
 [20] P. Adamson *et al.*, Nucl. Instrum. Meth. A **806**, 279 (2016).
 [21] P. Adamson *et al.* (MINOS), Phys. Rev. Lett. **101**, 221804 (2008).
 [22] P. Adamson *et al.* (MINOS), Phys. Rev. D **81**, 052004 (2010).
 [23] P. Adamson *et al.* (MINOS), Phys. Rev. Lett. **107**, 011802 (2011).
 [24] D. G. Michael *et al.* (MINOS), Nucl. Instrum. Meth. A **596**, 190 (2008).
 [25] C. Backhouse, D.Phil. Thesis, Oxford University (2011), FERMILAB-THESIS-2011-17.
 [26] R. Ospanov, Ph.D. Thesis, University of Texas at Austin (2008), FERMILAB-THESIS-2008-04.
 [27] P. Adamson *et al.* (MINOS), Phys. Rev. D **77**, 072002 (2008).
 [28] D. Hernandez and A. Yu. Smirnov, Phys. Lett. B **706**, 360 (2012).
 [29] G. L. Fogli *et al.*, Phys. Rev. D **86**, 013012 (2012).
 [30] F. P. An *et al.* (Daya Bay), Phys. Rev. Lett. **115**, 111802 (2015).
 [31] S.-H. Seo (RENO), AIP Conf. Proc. **1666**, 080002 (2015).
 [32] J. I. Crespo-Anadon (Double Chooz), Nucl. Part. Phys. Proc. **265–266**, 99 (2015).
 [33] A. Palazzo, Mod. Phys. Lett. A **28**, 1330004 (2013).
 [34] A. V. Devan, Ph.D. Thesis, College of William and Mary (2015), FERMILAB-THESIS-2015-12.
 [35] G. J. Feldman and R. D. Cousins, Phys. Rev. D **57**, 3873 (1998).
 [36] K. Abe *et al.* (Super-Kamiokande), Phys. Rev. D **91**, 052019 (2015).
 [37] F. Dydak *et al.* (CDHSW), Phys. Lett. B **134**, 281 (1984).
 [38] I. E. Stockade *et al.* (CCFR), Phys. Rev. Lett. **52**, 1384 (1984).
 [39] K. B. M. Mahn *et al.* (MiniBooNE and SciBooNE), Phys. Rev. D **85**, 032007 (2012).
 [40] P. Adamson *et al.* (Daya Bay and MINOS), (2016), submitted to Phys. Rev. Lett., arXiv:1607.01177 [hep-ex].

Note Added: Following completion of this manuscript, a paper submitted by the IceCube Collaboration that sets limits using sterile-driven disappearance of muon neutrinos has been accepted for publication (see arXiv:1605.01990 [hep-ex]). The results place strong constraints on $\sin^2 2\theta_{24}$ for $\Delta m_{41}^2 \in (0.1, 10)$ eV². Further, a paper that re-analyses the same IceCube data in a model including non-standard neutrino interactions has also been accepted for publication (see arXiv:1602.08766 [hep-ex]).